substance: boron compounds with group III elements
property: properties of boron-yttrium compounds: YB_{66}

Structure: cubic

Space group: Fm3c [69R, 97H].

Crystal chemistry of YB_{66} and $YB_{41}Si_{1.2}$ [99H].

A simplified schematic representation of the structure is shown in Fig. 1.

lattice parameter
(in Å)

a	23.440(6)	*T* = 300 K	YB_{66}, X-ray diffraction,	97H
	23.4364(6)		YB_{62}	
	23.4600(9)		YB_{56}	
	23.4...23.5	*T* = 300 K	X-ray diffraction, electron microscopy	76K, 77S

The structure (Fig. 2) contains giant $(B_{12})_{13}$ icosahedra (Fig. 3), B_{80} clusters (Fig. 4), and Y-Y pairs. All the sites of the non-icosahedral B_{80} cluster are partially occupied, thus the cluster contains about 42 B atoms only. In total, there are 1584 B atoms and 24 Y atoms per unit cell. The majority of the B atoms (1248) belongs to eight $(B_{12})_{13}$, and the remaining 336 B atoms form the non-icosahedral B_{80} cages, which are accommodated in the large holes resulting from the arrangement of the giant icosahedra. The Y atoms are statistically distributed over 48 sites per unit cell with 0.5 occupancy [97H].

In early publications the homogeneity range was said to be YB_n ($100 > n > 20$) [69R, 75B1, 76K, 77S]. Recent results show that single crystals of highest quality can be obtained for the compounds YB_{56} and YB_{62} [93K, 94T].

Preparation of single crystals with a floating zone method [85T, 86T1].

Growth of high quality single crystals [90T].

Floating zone growth of monochromator grade crystals of YB_{66} [93K].

Direct observation of $(B_{12})_{13}$ supericosahedra in [96P].

AFM pictures of cleaved YB_{66} surfaces [96K].

Atomic structures of YB_{56} studied by digital high-resolution electron microscopy and electron diffraction [99O].

Physical properties

Electronic structure and properties

For the discussion of the electronic properties of YB_{66} the new structure determination [97H] is essential. In particular must be taken into account that the B_{48} units, which were previously assumed to be largely compact clusters, in reality consist of 80 boron sites, all of which are occupied at about 50 % only. Hence in this unit a considerable content of unsaturated bonds exist, which may influence the electronic properties decisively and could be the reason for the similarity of the electronic properties to those of amorphous semiconductors.

Density of states calculations for the B_{156} framework, B_{48} and B_{36} clusters, and addition to that of the whole structure in Fig. 5 [94B].

B K_α spectrum in Fig. 6 [94G2].

energy gap
(in eV)

E_g	2.73	T = 180...280 K	sum of opt. and therm. excitation energy	97S1
	0.8	T > 500 K	estimated from el. cond.	77S
	1.0		derived from el. cond.	87G
	0.8	T > 500 K	electrical conductivity (estimated from Fig. 7; $YB_{61.5}$)	77S

critical points of YB_{52} in the interband transition range obtained from structure-modulated reflectivity spectra
(energy in eV)

E_{crit}	1.42	T = 300 K	YB_{52} used for reference	99W
	1.50			
	1.57			
	2.43			
	2.64			
	2.80			
	3.08			
	3.39			
	3.67			
	3.78			
	4.08			
	4.32			
	4.57			
	4.81			
	5.19			
	5.99			

Optical absorption edge spectrum in Fig. 8 [94K2].

Absorption edge also in [87W1].

thermal excitation energy of photoconduction

E	0.19 eV	T = 180...280 K	97S1

Amplitude and phase shift of the modulated photoconductivity depending on the modulation frequency in Fig. 9 [97S1].

binding energies
(in eV)

E_b	187.8(2)	B(1s)	97P
	157.1(2)	Y(3d) (+3 oxydation state)	
	159.1(2)	Y(3d) (+3 oxydation state)	

Impurities and defects

Effects of transition metal element (Cu, Ni) doping in YB_{66} [99T].

Lattice properties

elastic moduli

c_{11}	$3.80(3)\cdot10^{12}$ dyn cm^{-2}	T = 300 K,	from longitudinal-wave sound	77S
c_{44}	$1.60(8)\cdot10^{12}$ dyn cm^{-2}	ν = 60 MHz	velocity	
c_{12}	$0.4(5)\cdot10^{12}$ dyn cm^{-2}		derived value	

sound velocity

v_t	$7.89\cdot10^5$ cm s^{-1}		YB_{66}	71S
	$8.54\cdot10^5$ cm s^{-1}		YB_{63}, from torsion	94M
v_1	$1.18\cdot10^6$ cm s^{-1}	T = 300 K		77S

Temperature dependent change of the transverse sound velocity in Fig. 10 [94M].

electrical conductivity
(in Ω^{-1}cm^{-1})

σ	10^{-2}	T = 300 K		77S
	$3\cdot10^{-2}$	T = 300 K		86G
	$4\cdot10^{-6}$	T = 300 K		87W2
	$7\cdot10^{-3}$	T = 300 K		87G
	$1.5\cdot10^{-4}$	T = 300 K		94G1

Temperature dependence of the dc electrical conductivity in Fig. 11 [87W2, 91W].

Temperature dependence of the ac electrical conductivity in Fig. 12 [90W].

For temperature dependence of the electrical conductivity see also [94G1].

resistivity

ρ	$3.6\cdot10^2$ Ω cm	T = 300 K	For temperature dependence, see Fig. 7	77S

activation energies

E_A	0.3 eV	T = 500 K	derived from Hall effect	91W
	1.00 eV		derived from electrical conductivity	87G

Hall mobility

μ_H	$5\cdot10^{-2}$...2 cm^{2}V^{-1}s^{-1}		T = 300 K	91W

Temperature dependence of the Hall mobility in Fig. 13 [91W].

thermoelectric power
(in μV K^{-1})

S	850	T = 300 K		91W
	340	T = 300 K		87G
	780	T = 300 K		94G1

Thermoelectric power in Fig. 14 [87W2, 91W].

For the temperature dependence of the thermoelectric power see also [94G1].

magnetoresistance

$\Delta\rho/\rho$	$1\cdot10^{-4}$	T = 300 K	B = 1 T	91W

Temperature dependence of the magnetoresistance in Fig. 15 [91W].

resonance frequencies of IR-active phonons of YB_{66} at different temperatures
(uncertain data in parantheses)
(ν/c in cm^{-1})

30 K	160 K	300 K	450 K	
	31	29	30	94K1
	73	72	72	

			100
112	(114)	(116)	113
137	133	131	131
163	165	164	164
195	189	189	187
238			
254			
272	273	273	276
291			
327	334	338	345(5)
341	(344)	(352)	(362)
363			
380	379		(389)
399	402	402	(400)
413	(418)	(418)	(417)
436	433		
			476
487	489	488	488(5)
507	(507)	(507)	(511)
523	(527)	(524)	(525)
	(581)	(575)	(581)
596	598	598	600
	644	633	635
673(10)	677(10)	673(10)	667(10)
(783)	(787)	(781)	(773)
847	845	843	845
907	907	905	903
986(5)	988(5)	984(5)	984(5)
1026(10)	1030(10)	1022(10)	1022(10)
1146(5)	1148(5)	1140(5)	1144(10)

IR absorption spectra of YB_{66} at different temperatures in the range of phonon frequencies in Fig. 16 [94K2, 94K1].

Absorption index in [91W].

IR reflectivity spectra showing the influence of dynamical conductivity at low wavenumbers in Fig. 17 [96S]. See also [97S3, 98S].

IR reflectivity spectra in [87W1, 87W2, 91W, 94K1, 94K3].

FT Raman spectrum of YB_{66} in Fig. 18 [94K2; 94K1, 91W].

far infrared optical absorption: see Fig. 19

refractive indices

n_∞	3.19	T = 300 K	from interferences in opt. spectra	94K2
n_0	3.66	T = 300 K	from interferences in opt. spectra	
Δn	0.47		error of sample thickness eliminated	94K1

dielectric constants

ε_∞	10.2	T = 300 K	from interferences	94K2
ε_0	13.38	T = 300 K	from interferences	
$\Delta\varepsilon$	3.18		error of sample thickness eliminated	94K1

thermal conductivity

κ	2...3·10^{-2} W cm^{-1}K^{-1}		T = 300 K	87C, 91M
	≈ 20·10^{-3} W cm^{-1} K^{-1}	T = 300 K		71S
	0.58 W cm^{-1} K^{-1}		computed value for T = 0 K For temperature dependence, see Fig. 20	71S

Temperature dependence of the thermal conductivity of different compositions in Fig. 21. [71S, 77S, 87C, 89C, 92R, 94M].

Thermal conductivity of YB_{66} and YB_{61} in [86T2], of $YB_{61.7}$ and YB_{66} (results of different authors) in [94M], of YB_{63} in [98M], of YB_{58} and YB_{66} in [87C, 89C, 91M].

phonon mean free path

Λ	$23.44 \cdot 10^{-8}$ cm	T = 300 K	For temperature dependence, see Fig. 22	71S

Heat capacity in Fig. 23 [87C, 89C].

Dependence of the specific heat capacity divided by T^3 on temperature in Fig. 24 [87C, 74B, 75B1].

For specific heat (comparison of different samples) see also [91M].

For a comparison of the thermal conductivity with numerous amorphous solids and disordered crystals see [97M].

Debye temperature

Θ_D	1300(50) K	~	calculated from elastic constants	71S, 77S
	1200 K		heat capacity (preliminary measurements)	77S

density

d	2.568 g cm^{-3}	T = 300 K	YB_{66}	94M
	2.5687(50) g cm^{-3}	T = 300 K	pycnometric	77S, 71S
	2.482 g cm^{-3}	T = 300 K	X-ray	71S

acoustic phonon cutoff

	80 cm^{-1}	71S

acoustic attenuation: see Fig. 25.

melting point

T_m	2100°C	77S

internal friction

Q^{-1}	$1.7 \cdot 10^{-4}$	T = 10 K	YB_{66}	94M
	$7 \cdot 10^{-4}$		$YB_{61.7}$	
	$2.2 \cdot 10^{-4}$		YB_{63}	

Temperature dependence of the internal friction of YB_{66}, YB_{63} and $YB_{61.7}$ in Fig. 26 [94M].

Structure and chemistry of the YB_{66} (100) surface in [97P]; surface reconstruction determined by AFM investigation [96K].

Application of YB_{66} single crystals for monochromators of synchrotron radiation in [94T].

References:

69R Richards, S.M., Kasper, J.S.: Acta Crystallogr. B 25 (1969) 237.

71S Slack, G. A., Oliver, D. W., Horn, E. H.: Phys. Rev. B 4 (1971) 1714.

74B Bilir, N.: in: Ph.D. Thesis, Stanford University ed., Stanford, 1974 .

75B1 Benesovsky, F.: Ullmanns Enzyklopädie der techn. Chemie 8 (1975) 657.

75B2 Bilir, N., Phillips, W.A., Geballe, T.H.: in: Low Temperature Physics LT 14, M. Krusius and M. Vuorio ed., North-Holland: Amsterdam, 1975, p. 9.

76K Kasper, J. S.: J. Less-Common Met. 47 (1976) 17.

77S Slack, G. A., Oliver, D. W., Brower, G. D., Young, J. D.: J. Phys. Chem. Solids 38 (1977) 45.

85T Tanaka, T., Otani, S., Ishizawa, Y.: J. Cryst. Growth 73 (1985) 31.

86G Golikova, O.A., Tadzhiev, A.: J. Non-Cryst. Solids 87 (1986) 64.

86T1 Tanaka, T., Otani, S., Ishizawa, Y.: J. Less-Common Met. 117 (1986) 293 (Proc. 8th Int. Symp. Boron, Borides, Carbides, Nitrides and Rel. Compounds, Tbilisi, Oct. 8 - 12, 1984).

86T2 Türkes, P.R.H., Swartz, E.T., Pohl, R.O.: in: Boron-Rich Solids (AIP Conf. Proc. 140), Albuquerque, New Mexico 1985, D. Emin, T.L. Aselage, C.L. Beckel, I.A. Howard ed., American Institute of Physics: New York, 1986, p. 346.

87C Cahill, D.G., Fischer, H.E., Warson, S.K., Pohl, R.O., Slack, G.A.: in: Proc. 9th Int. Symp. Boron, Borides and Rel. Compounds, University of Duisburg, Germany, Sept. 21 - 25, 1987, H. Werheit ed., University of Duisburg: Duisburg, 1987, p. 113.

87G Golikova, O.A.: Phys. Status Solidi (a) 101 (1987) 277.

87W1 Werheit, H.: in: Proc. 9th Int. Symp. Boron, Borides and Rel. Compounds, University of Duisburg, Germany, Sept. 21 - 25, 1987, H. Werheit ed., University of Duisburg: Duisburg, 1987, p. 142.

87W2 Werheit, H., Haupt, H., Kuhlmann, U., Siejak, V., Tanaka, T.: in: Proc. 9th Int. Symp. Boron, Borides and Rel. Compounds, University of Duisburg, Germany, Sept. 21 - 25, 1987, H. Werheit ed., University of Duisburg: Duisburg, 1987, p. 383.

89C Cahill, D.G., Fischer, H.E., Watson, S.K., Pohl, R.O., Slack, G.A.: Phys. Rev. B 40 (1989) 3254.

90T Tanaka, T., Otani, S., Ishizawa, Y.: J. Cryst. Growth 99 (1990) 994.

90W Werheit, H., Kuhlmann, U., Tanaka, T.: (unpublished results).

91M Medwick, P.A., Cahill, D.G., Raychaudhuri, A.K., Pohl, R.O, Gompf, F., Nücker, N., Tanaka, T.: in: Boron-Rich Solids, Proc. 10th Int. Symp. Boron, Borides and Rel. Compounds, Albuquerque, NM 1990 (AIP Conf. Proc. 231), D. Emin, T.L. Aselage, A.C. Switendick, B. Morosin, C.L. Beckel ed., American Institute of Physics: New York, 1991, p. 363.

91W Werheit, H., Kuhlmann, U., Tanaka, T.: in: Boron-Rich Solids, Proc. 10th Int. Symp. Boron, Borides and Rel. Compounds, Albuquerque, NM 1990 (AIP Conf. Proc. 231), D. Emin, T.L. Aselage, A.C. Switendick, B. Morosin, C.L. Beckel ed., American Institute of Physics: New York, 1991, p. 125.

92R Raychaudhuri, A.K., Pohl, R.O.: Phys. Rev . B 46 (1992) 10657.

93K Kamimura, Y., Tanaka, T., Otani, S., Ishizawa, Y., Rek, Z.U., Wong, J.: J.Cryst. Growth 128 (1993) 429.

94B Bullett, D.W.: Proc. 11th Int. Symp. Boron, Borides and Rel. Compounds, Tsukuba, Japan, August 22 - 26, 1993, Jpn. J. Appl. Phys. Series 10 (1994), p. 31.

94G1 Golikova, O.A.: Proc. 11th Int. Symp. Boron, Borides and Rel. Compounds, Tsukuba, Japan, August 22 - 26, 1993, Jpn. J. Appl. Phys. Series 10 (1994), p. 43.

94G2 Golikova, O.A., Domashevskaya, E.P., Kazanin, M.M., Terekhov, V.A.: Proc. 11th Int. Symp. Boron, Borides and Rel. Compounds, Tsukuba, Japan, August 22 - 26, 1993, Jpn. J. Appl. Phys. Series 10 (1994), p. 56.

94K1 Kuhlmann, U.: Zusammenhänge zwischen den Phononenspektren borreicher Festkörper mit Ikosaederstruktur und ihren strukturellen und elektronischen Eigenschaften, Thesis, Gerhard-Mercator University, Duisburg, Germany, 1994.

94K2 Kuhlmann, U., Werheit, H., Hassdenteufel, J., Tanaka, T.: Proc. 11th Int. Symp. Boron, Borides and Rel. Compounds, Tsukuba, Japan, August 22 - 26, 1993, Jpn. J. Appl. Phys. Series 10 (1994), p. 82.

94K3 Kobayashi, M., Higashi, I., Matsuda, H., Kimura, K.: J. Alloys Compounds 221 (1994) 120.

94M Medwick, P.A., Pohl, R.O., Tanaka, T.: Proc. 11th Int. Symp. Boron, Borides and Rel.Compounds, Tsukuba, Japan, August 22 - 26, 1993, Jpn. J. Appl. Phys. Series 10 (1994), p. 106.

94T Tanaka, T., Ishizawa, Y., Wong, J., Rek, Z.U., Rowen, M., Schäfers, F., Müller, B.R.: Proc. 11th Int. Symp. Boron, Borides and Rel. Compounds, Tsukuba, Japan, August 22 - 26, 1993, Jpn. J. Appl. Phys. Series 10 (1994), p. 110.

96K Kuhlmann, U., Werheit, H., Tanaka, T., Ishizawa, Y.: (presented at the 12th Int. Symp. Boron, Borides and Rel. Compounds, Baden, Austria, 1997.

96P Perkins, C.L., Trenary, M., Tanaka, T.: Phys. Rev. Lett. 77 (1996) 4772.

96S Schmechel, R., Werheit, H.: J. Phys.: Condens. Matter 8 (1996) 7263.

97H Higashi, I., Kobayashi, K., Tanaka, T., Ishizawa, Y.: J. Solid State Chem. 133 (1997) 16 (Proc. 12th Int. Symp. Boron, Borides and Rel. Compounds, Baden, Austria, 1996).

97M Medwick, P.A., Pohl, R.O.: J. Solid State Chem. 133 (1997) 44 (Proc. 12th Int. Symp. Boron, Borides and Rel. Compounds, Baden, Austria, 1996).

97P Perkins, C.L., Trenary, M., Tanaka, T.: J. Solid State Chem. 133 (1997) 31 (Proc. 12th Int. Symp. Boron, Borides and Rel. Compounds, Baden, Austria, 1996).

97S1 Sakairi, Y., Takeda, M., Kimura, K., Tanaka, T.: J. Solid State Chem. 133 (1997) 195 (Proc. 12th Int. Symp. Boron, Borides and Rel. Compounds, Baden, Austria, 1996).

97S2 Simeone, D., Deschanels, X., Berthier, B., Tessier, C.: J. Nucl. Mater. 245 (1997) 27.

97S3 Schmechel, R., Werheit, H.: J. Solid State Chem. 133 (1997) 335 (Proc. 12th Int. Symp. Boron, Borides and Rel. Compounds, Baden, Austria, Aug. 25 - 30, 1996).

98M Medwick, P.A., White Jr., B.E., Pohl, R.O.: J. Alloys Compounds 270 (1998) 1.

98S Schmechel, R.: Thesis, Gerhard-Mercator University Duisburg, Germany, 1998.

99H Higashi, I., Ishii, T., Kobayashi, K., Tanaka, T.: J. Solid State Chem. (2000) (Proc. 13th Int. Symp. Boron, Borides and Rel. Compounds, Dinard, France, Sept. 1999).

99O Oku, T., Bovin, J.-O., Higashi, I., Tanaka, T., Ishizawa, Y.: J. Solid State Chem. (2000) (Proc. 13th Int. Symp. Boron, Borides and Rel. Compounds, Dinard, France, Sept. 1999).

99T Tanaka, T., Shi, Y., Mori, T., Leithe-Jasper, A.: J. Solid State Chem. (2000) (Proc. 13th Int. Symp. Boron, Borides and Rel. Compounds, Dinard, France, Sept. 1999).

99W Werheit, H.: in: Electric Refractory Materials, Y. Kumashiro ed., Marcel Dekker: New York, 1999 (in press).

Fig. 1.

YB_{66}. Simplified schematic representation of the crystal structure looking down along the [100] axis. The horizontal and vertical directions are [010] and [001]. Different shading of the spheres representing B_{156} groups indicate different orientation. The B_{48} groups are situated at $a/4$, the Y atoms at 0.054 a below the surface. The Y sites are believed to be statistically occupied [77S].

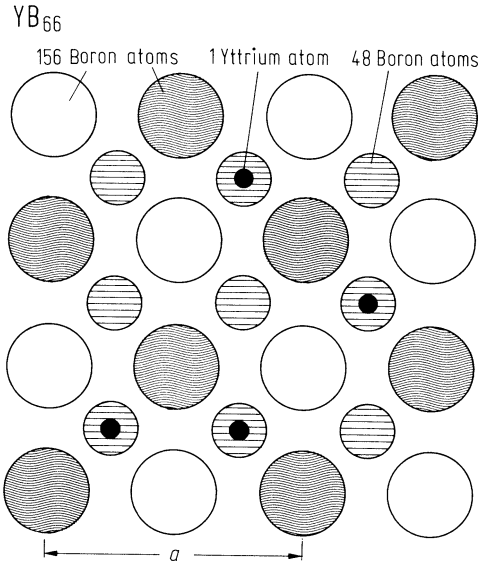

Fig. 2.

YB_{66} structure group. Structure containing $(B_{12})_{13}$ giant icosahedra, B_{80} clusters (80 B sites, about 42 of which are statistically occupied) and Y-Y pairs [97H].

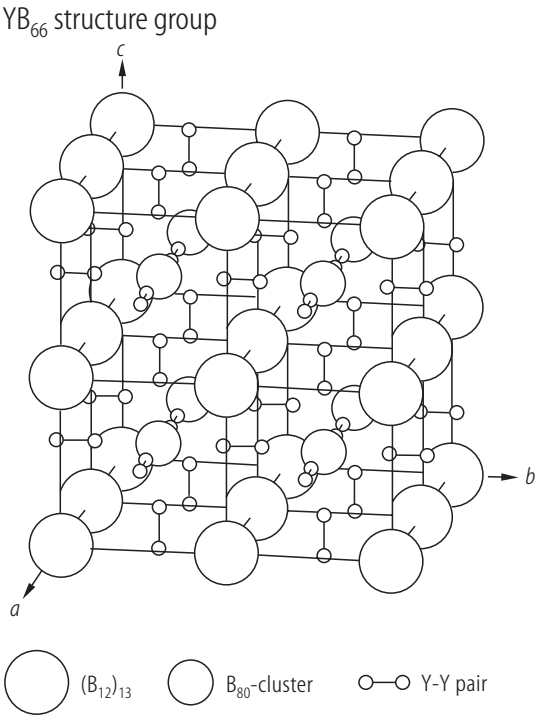

Fig. 3.

YB_{66}. Arrangement of the $(B_{12})_{13}$ units as seen along the *c* axis ($-0.25 < z < +0.25$) [97H].

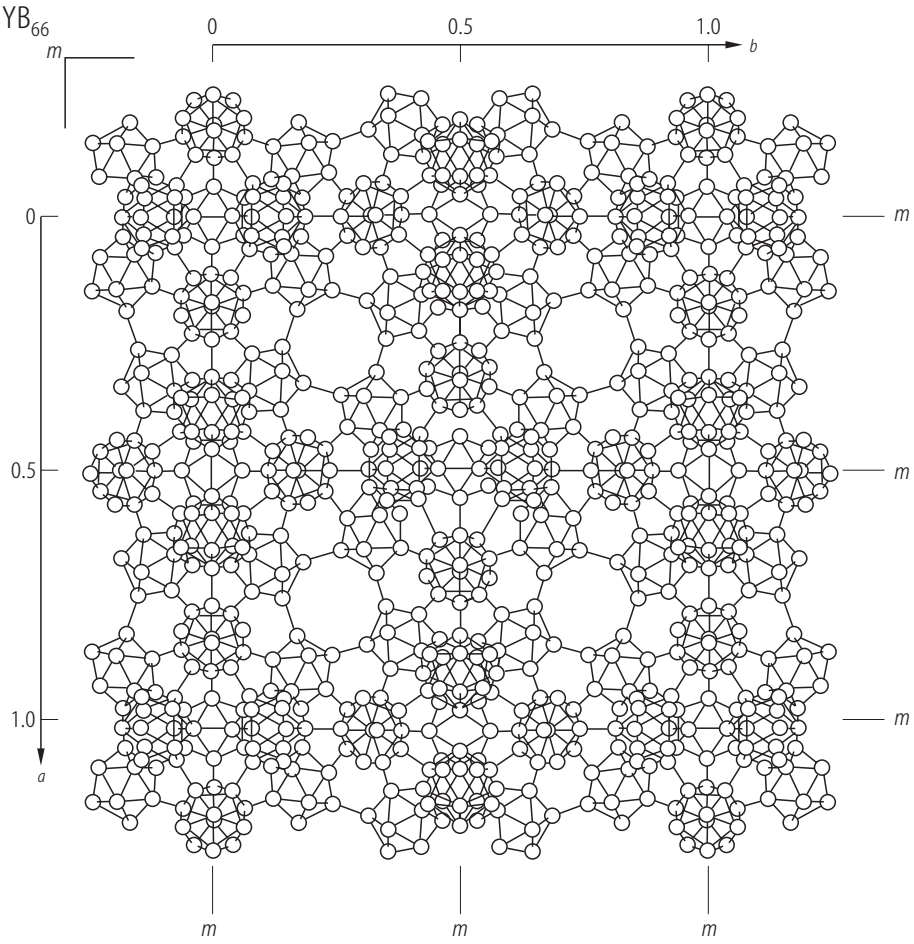

Fig. 4.

YB_{66}. B_{80} cluster as seen along the fourfold axis. The cluster consists of 80 B sites belonging to four crystallographically different positions. All the sites are partially occupied so that the actual number of B atoms within the cluster is about 42 [97H].

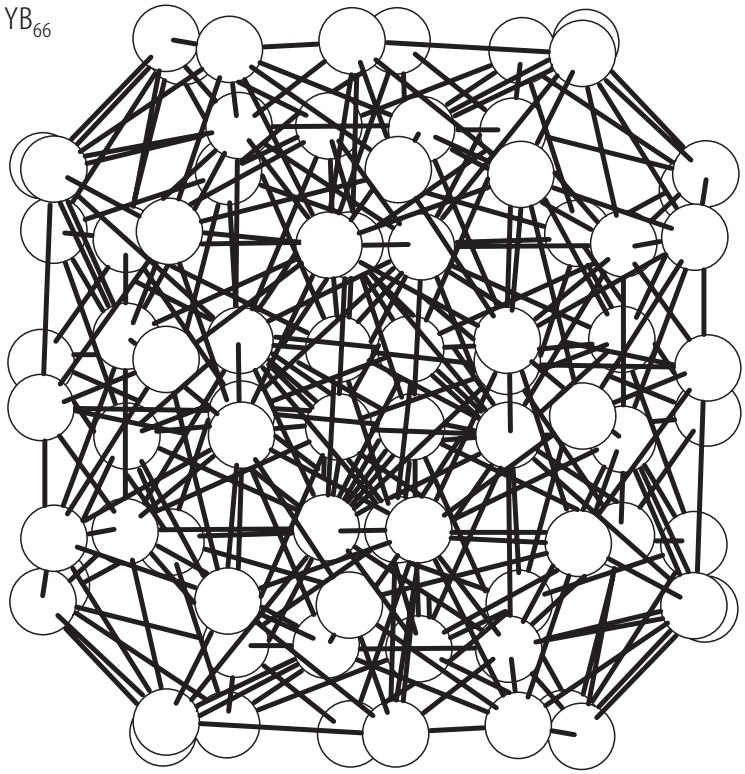

Fig. 5.

YB_{66}. Calculated electron density of states. **(a)** B_{156} framework, **(b)** assumed B_{48} cluster; **(c)** sum of B_{156} framework and B_{48} cluster, **(d)**) sum of B_{156} framework and an assumed B_{36}cluster [94B].

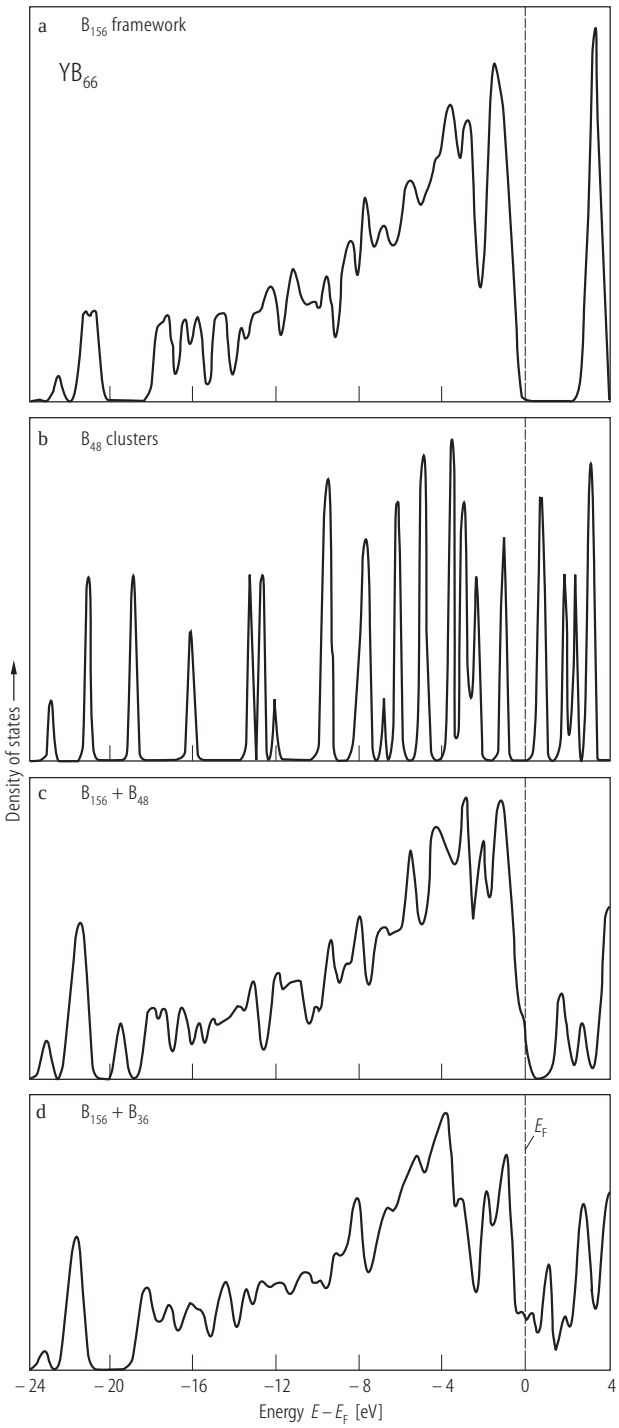

Fig. 6.

YB_{66}. B K_α spectrum; insert: high energy tail [94G2].

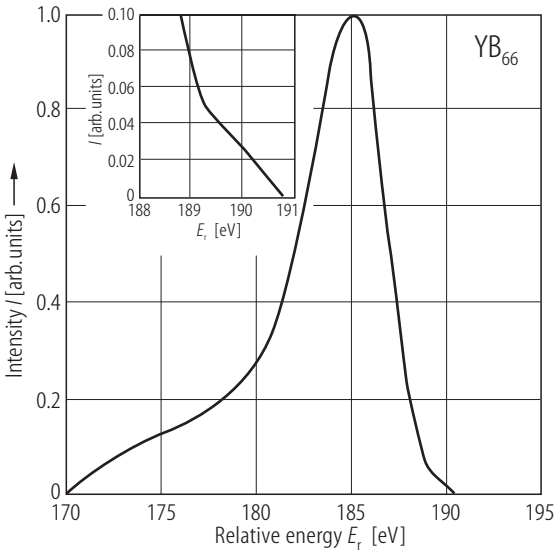

Fig. 7.

$YB_{61.5}$. Electrical resistivity vs. reciprocal temperature [77S].

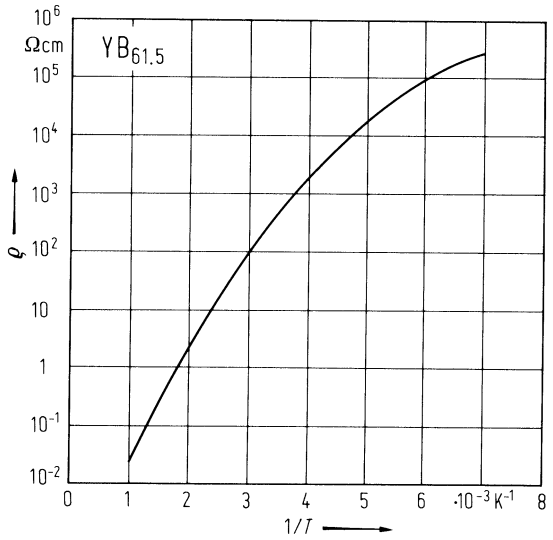

Fig. 8.

YB_{66}. Optical absorption edge; absorption coefficient vs. photon energy. The agreement between the results obtained with monochrome and polychrome radiation shows that the measured absorption is not remarkably influenced by photoeffect [94K2].

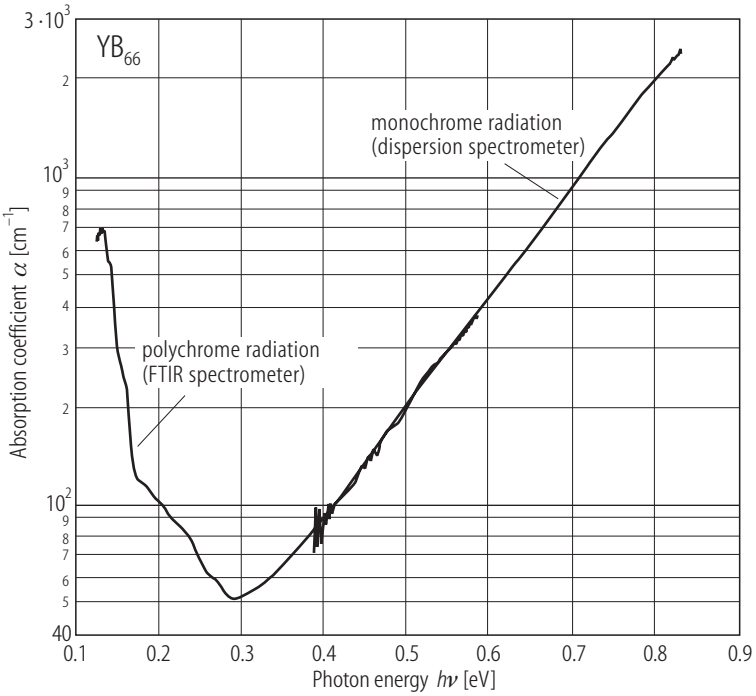

Fig. 9.

YB_{66}. Photoconductivity depending on the modulation frequency; **(a)** current, **(b)** phase shift [97S1].

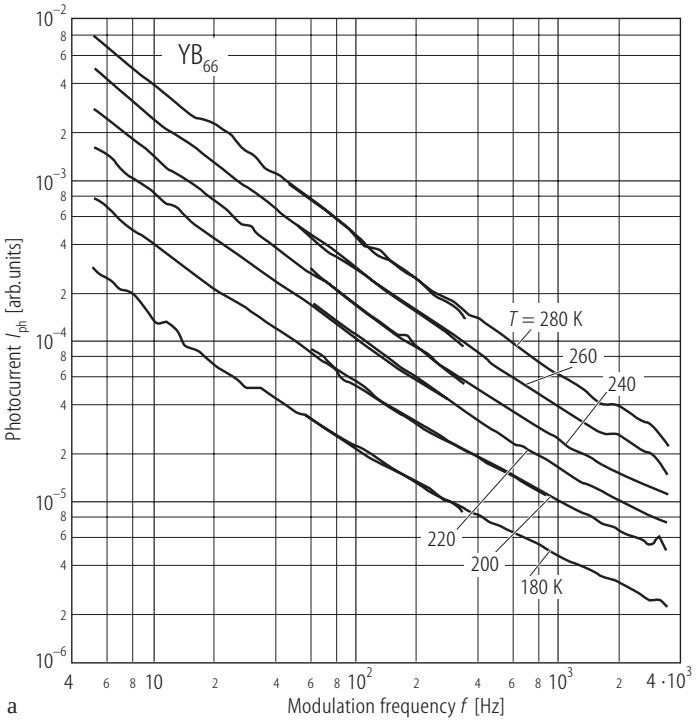

a

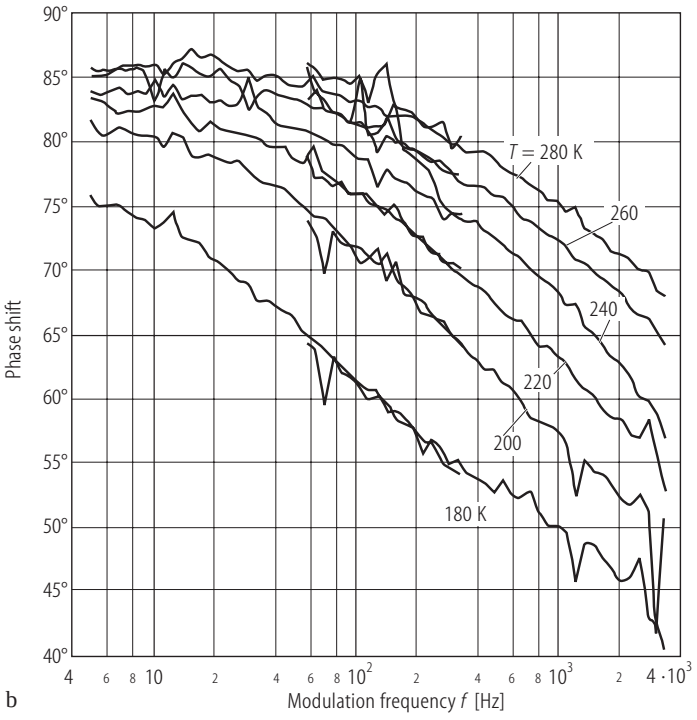

b

Fig. 10.

YB_{66}. Relative change of the transverse sound velocity of YB_{63} vs. T; solid line, calculation based on specific assumptions on the slope of $\delta v/v$ vs. T at intermediate temperatures ($\delta v/v = C \ln T$ for $T << T_{c0}$; $\delta v/v = -C/2 \ln T$ for $T >> T_{c0}$) (for details see ref.) [94M].

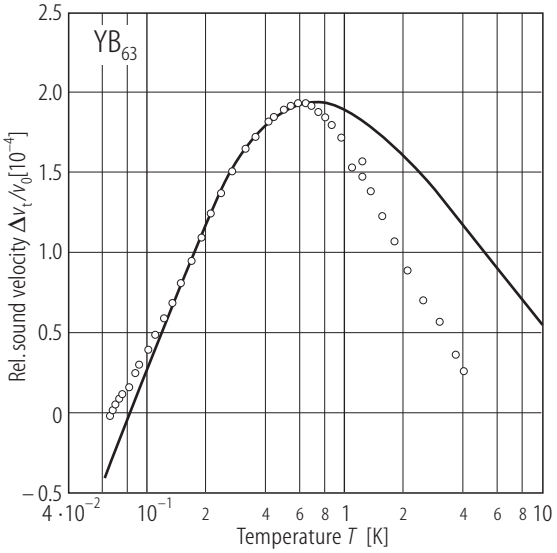

Fig. 11.

YB_{66}, DyB_{66}. dc electrical conductivity; σ vs. reciprocal T. Insert $\sigma T^{1/2}$ vs. $T^{-1/4}$ (Mott's law). Sample a: single crystal, double zone-melted; sample b: single crystal, zone melted; sample c: polycrystalline, industrial production [91W].

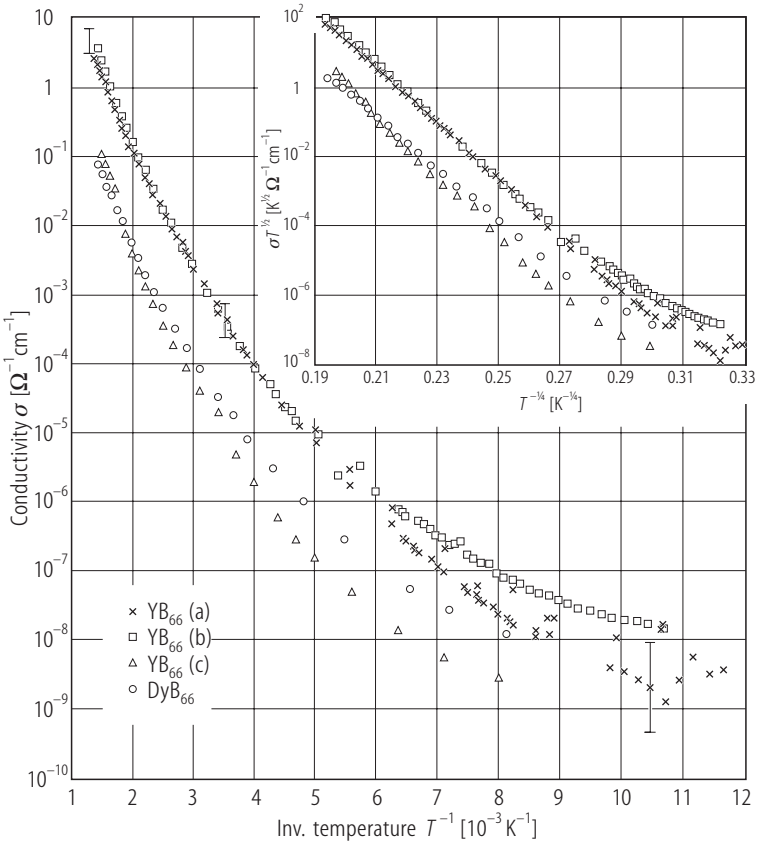

Fig. 12.

YB_{66}. ac electrical conductivity up to 2016 Hz [90W].

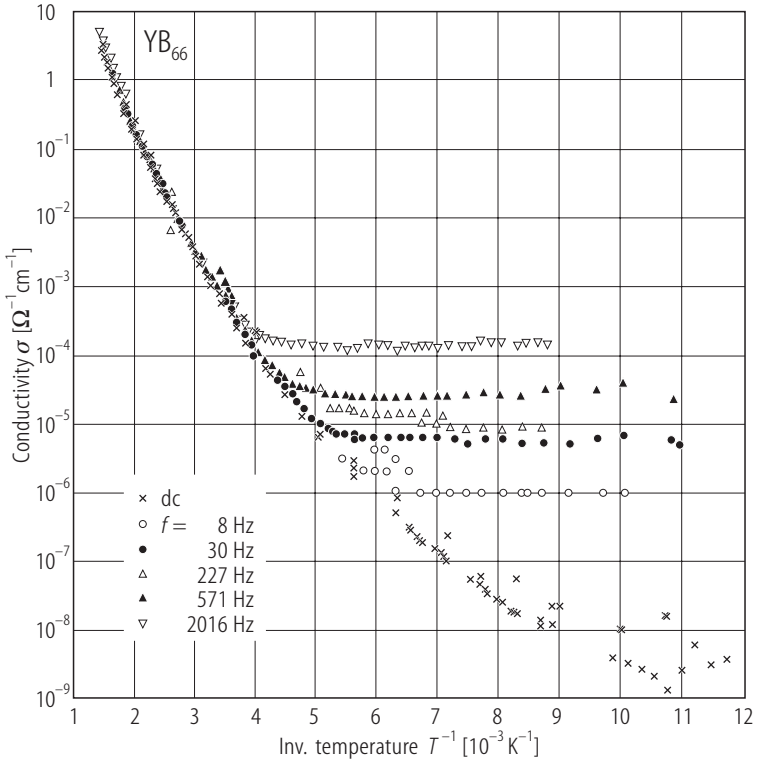

Fig. 13.

YB_{66}. Hall mobility vs. reciprocal *T*. Sample a: single crystal, double zone-melted; sample b: single crystal, zone melted; sample c: polycrystalline, industrial production [91W].

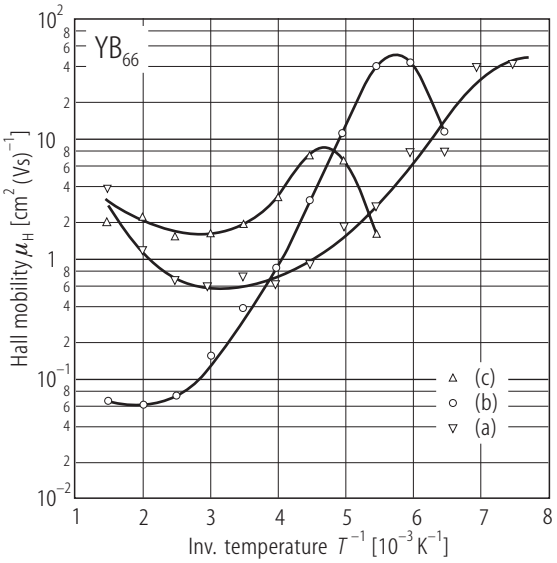

Fig. 14.

YB_{66}. Thermoelectric power S vs. T [91W].

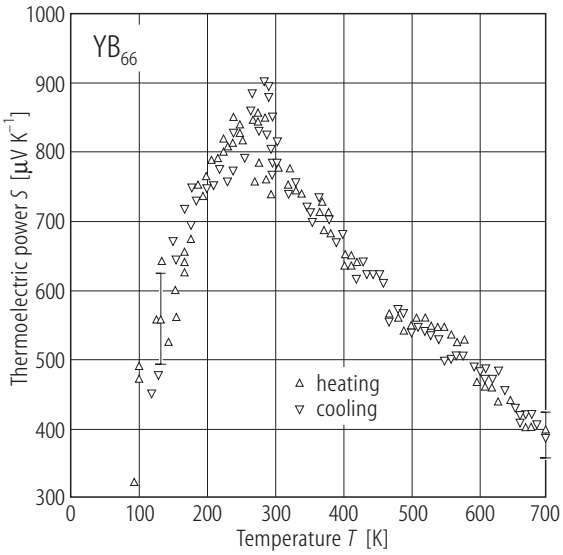

Fig. 15.

YB_{66}. Magnetoresistance $\Delta\rho/\rho$ vs. reciprocal T (B = 1 T) Squares: negative sign, open circles: positive sign [91W].

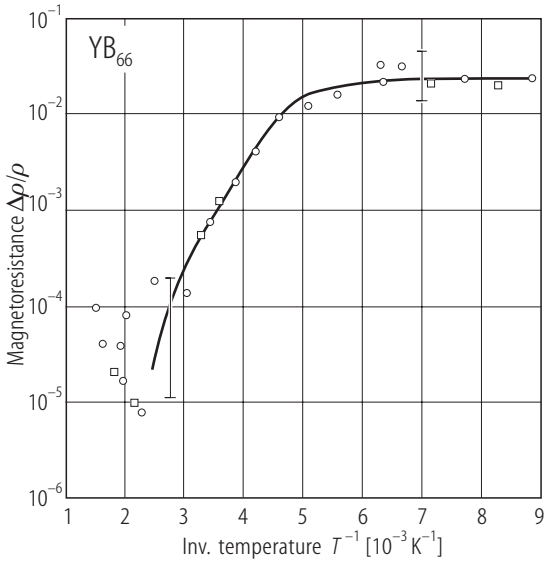

Fig. 16.

YB_{66}. Absorption index vs. wavenumber for 30, 160, 300, and 450 K [94K1, 94K2].

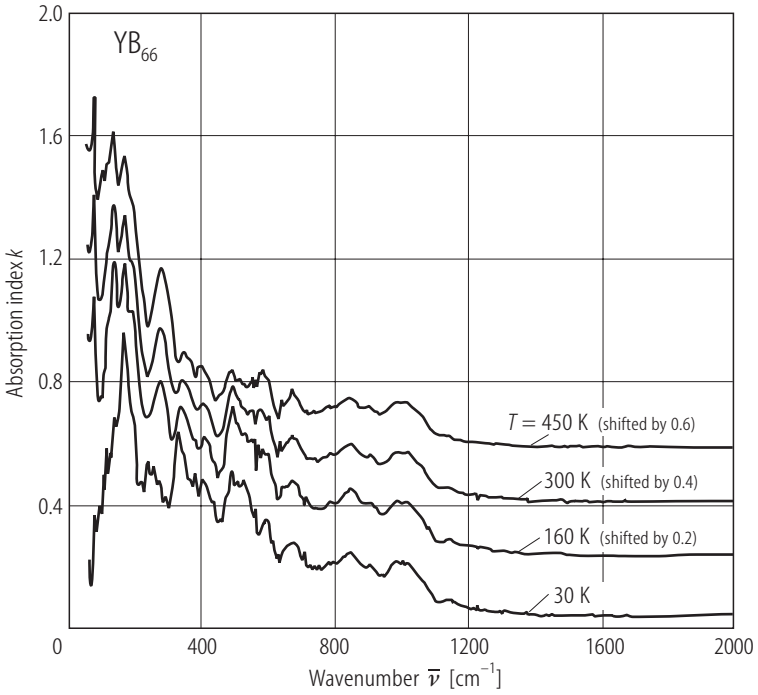

Fig. 17.

YB_{66}.Reflectivity spectra at 90, 300, and 450 K. The influence of the dynamical conductivity increasing with increasing temperature is clearly seen at low wavenumbers [98S].

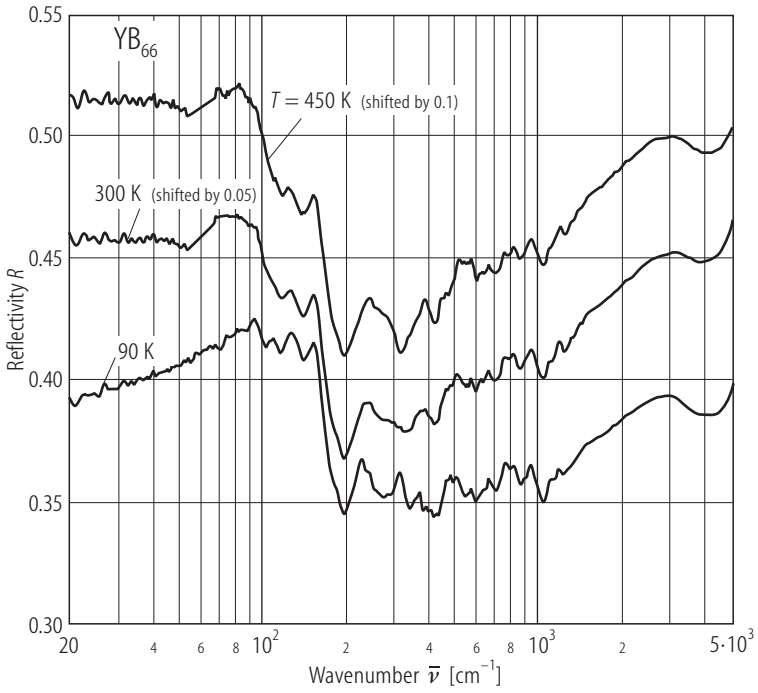

Fig. 18.

YB_{66}. Typical FT Raman spectra averaged over different numbers of scans [94K2].

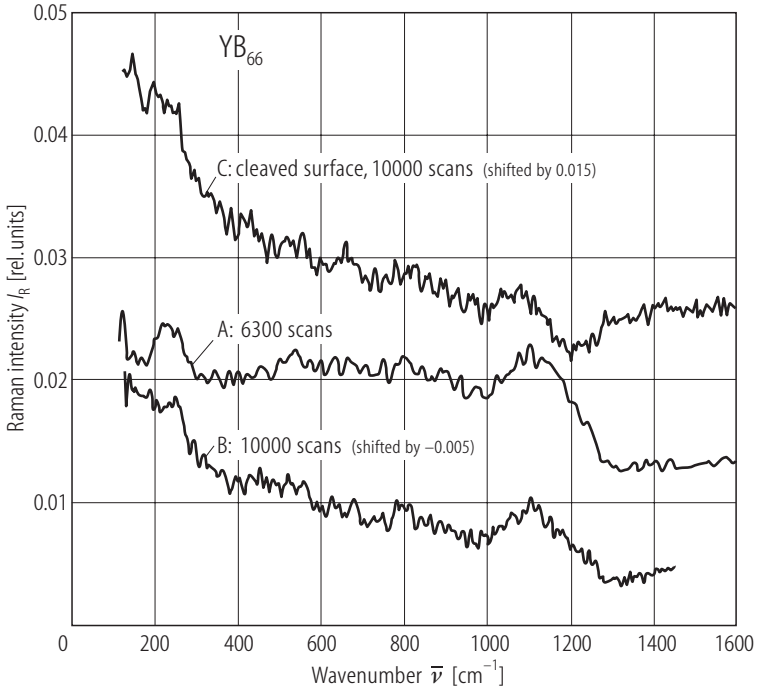

Fig. 19.

YB_{66}. Far infrared optical absorption coefficient at 4.2 K vs. wavenumber [77S].

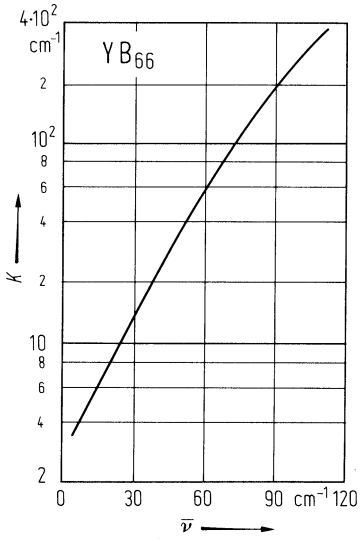

Fig. 20.

YB_{66}. Thermal conductivity vs. temperature for two samples [71S].

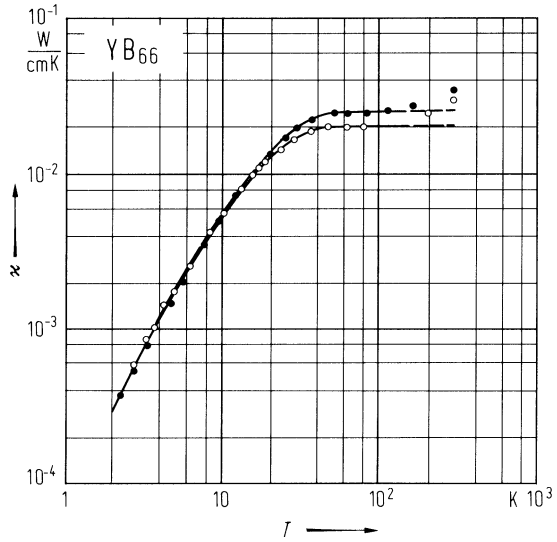

Fig. 21

YB_{66} structure group. Temperature dependence of thermal conductivity. Open symbols: $YB_{66\pm X}$ (squares, $YB_{61.7}$ [92R, 94M]; triangles, YB_{66} [71S, 94M], circles, YB_{66} [87C, 89C, 94M], diamonds, YB_{66} [77S, 94M]); closed symbols: $GdB_{66\pm X}$ (circles, GdB_{66} [86G], triangles down, $GdB_{62.5}$ [94M]).

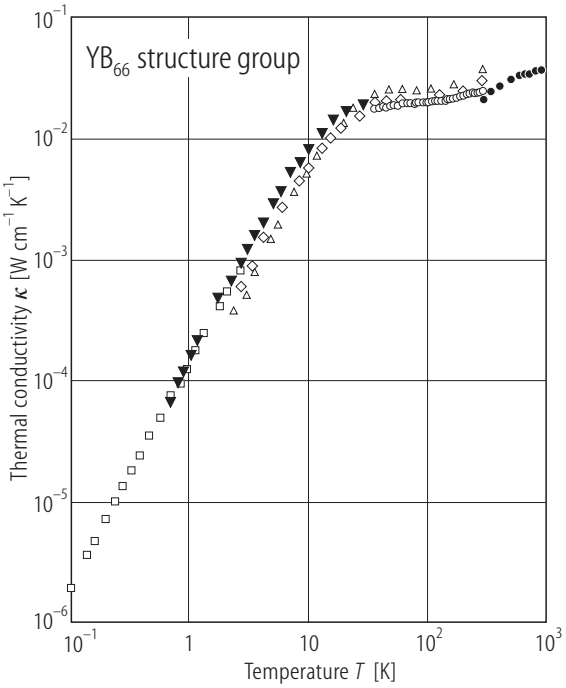

Fig. 22.

YB_{66}. Phonon mean free path vs. temperature [71S]. The dashed line represents the behavior of the acoustic phonons only and corresponds to the mean free path of the actual carriers with thermal energy.

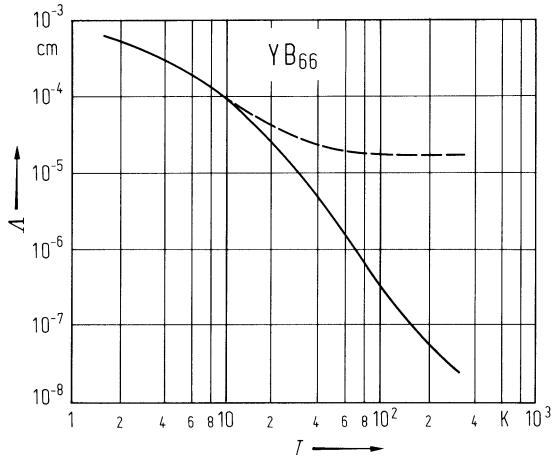

Fig. 23.

YB_{66}. Specific heat capacity c vs. T. Insert: Low temperature c/T vs. T^2, dashed line: Debye prediction [87C, 89C].

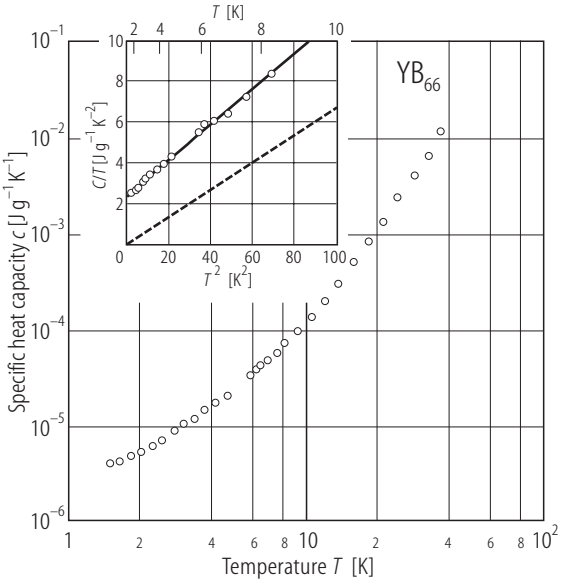

Fig. 24.

YB_{66}. Specific heat capacity divided by T^3 vs. T. Full circles:YB_{66} [87C], open circles: YB_{66} [74B, 75B2], crosses:$YB_{61.7}$ [74B, 75B2], dashed line, Debye model.

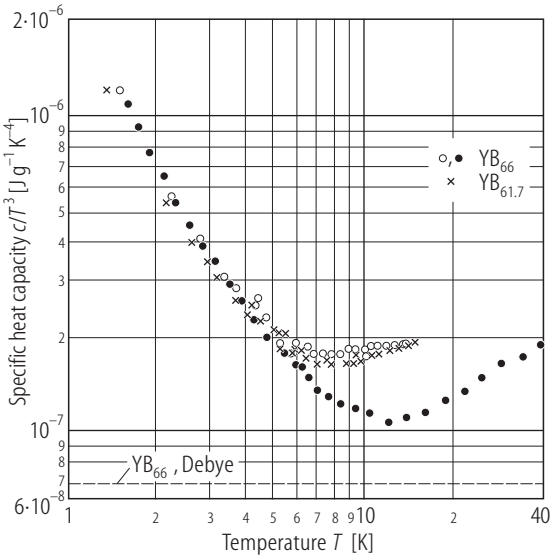

Fig. 25.

$YB_{61.7}$, YB_{66}. Acoustic attenuation α vs. temperature for transverse waves propagating in the [100] direction at different frequencies. At a frequency of 1.15 GHz the attenuation becomes unmeasurably large at temperatures above 11 K [77S]

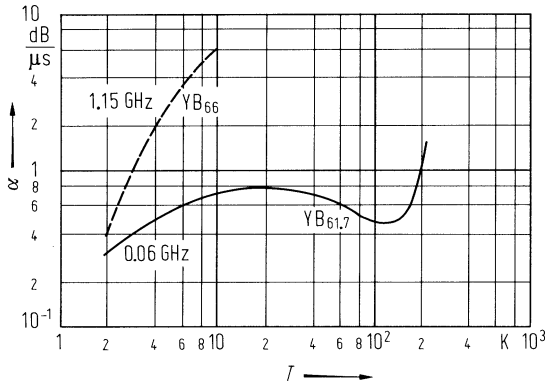

Fig. 26.

YB_{66}, $GdB_{62.5}$. Internal friction Q^{-1} vs. T for YB_{66}, YB_{63}, $YB_{61.7}$ and $GdB_{62.5}$ [94M].